Journal of Power Sources 196 (2011) 2211–2220

Contents lists available at ScienceDirect

Journal of Power Sources

journal homepage: www.elsevier.com/locate/jpowsour

Lithium diffusion in $Li_4Ti_5O_{12}$ at high temperatures

M. Vijayakumar, Sebastien Kerisit, Kevin M. Rosso, Sarah D. Burton, Jesse A. Sears, Zhenguo Yang, Gordon L. Graff, Jun Liu, Jianzhi Hu*

Pacific Northwest National Laboratory, Richland, WA 99352, USA

ARTICLE INFO

Article history:
Received 20 July 2010
Received in revised form 8 September 2010
Accepted 20 September 2010
Available online 29 September 2010

Keywords:
Lithium battery
Anode materials
6Li NMR
Molecular dynamics

ABSTRACT

Synthesis of the spinel lithium titanate $Li_4Ti_5O_{12}$ by an alkoxide-free sol–gel method is described. This method yields highly pure and crystalline $Li_4Ti_5O_{12}$ samples at relatively low temperature (850 °C) and via short thermal treatment (2 h). ^{6}Li magic angle spinning nuclear magnetic resonance (MAS NMR) measurements on these samples were carried out at high magnetic field (21.1 T) and over a wide temperature range (295–680 K). The temperature dependence of the chemical shifts and integral intensities of the three ^{6}Li resonances demonstrates the migration of lithium ions from the tetrahedral 8*a* to the octahedral 16*c* sites and the progressive phase transition from a spinel to a defective NaCl-type structure. This defective structure has an increased number of vacancies at the 8*a* site, which facilitate lithium diffusion through $16c \rightarrow 8a \rightarrow 16c$ pathways, hence providing an explanation for the reported increase in conductivity at high temperatures. Molecular dynamics simulations of the spinel oxides $Li_{4+x}Ti_5O_{12}$, with $0 \leq x \leq 3$, were also performed with a potential shell model in the temperature range 300–700 K. The simulations support the conclusions drawn from the NMR measurements and show a significant timescale separation between lithium diffusion through 8*a* and 16*c* sites and that out of the 16*d* sites.

1. Introduction

Titanium oxide polymorphs have received much attention due in part to their application in solid-state lithium-ion batteries [1–3]. In particular, spinel-structured lithium titanates have shown promising properties for use as electrode materials [4,5]. For example, the spinel $Li_4Ti_5O_{12}$ ($Fd\bar{3}m$) is being considered as a potential anode material for commercial purposes due to its excellent electrochemical properties, which include a low reduction potential (~1.5 V vs. Li/Li^+), high reversibility of the Li^+ insertion/extraction process, and a flat operating voltage [6]. In addition, this material undergoes minimal structural changes upon lithium insertion and extraction and has been termed a zero-strain insertion material [6,7]. Indeed, in-situ energy dispersive X-ray diffraction shows that variations in lattice parameters upon lithium insertion and extraction are at most 1% [8]. Finally, $Li_4Ti_5O_{12}$ can be charged up to $Li_7Ti_5O_{12}$, which corresponds to a theoretical capacity of 175 mA h g^{-1}, and shows an excellent capacity maintenance ratio of 99% even after the 100th cycle [9]. It should be noted that it has been suggested based on both experimental [10,11] and computational [12] results that further lithium can be inserted in $Li_7Ti_5O_{12}$ up to a stoichiometry of $Li_9Ti_5O_{12}$ at a potential of less than 1 V, resulting in a theoretical capacity of 293 mA h g^{-1}. These excellent electrochemical properties make this material a prime candidate for use as anode material in commercial lithium-ion batteries [13].

The use of $Li_4Ti_5O_{12}$ in commercial devices will be facilitated by a synthesis method that can easily be implemented for bulk production. However, the synthesis techniques reported to date, such as solid-state synthesis [6,14,15], sol–gel [16,17], combustion technique [18,19], rheological phase reaction [20] and ball milling method [15,21], for preparing $Li_4Ti_5O_{12}$ use excessive heat treatment (>850 °C and >12 h) and/or highly toxic and air sensitive starting materials, which complicates their use in industrial environments. In this report, we present a simple sol–gel method using water and a soluble titanium citrate complex as starting material, which helps to prepare $Li_4Ti_5O_{12}$ in open air and relatively short heat treatment (2 h).

The attractive electrochemical properties of $Li_4Ti_5O_{12}$ arise mainly from the lithium diffusion behavior in its crystal lattice. Considerable efforts have been made to understand lithium diffusion and local structure in $Li_4Ti_5O_{12}$. The crystal structure of $Li_4Ti_5O_{12}$ was initially reported by Deschanvres et al. [22] and subsequently by Kataoka et al. [23]. The latter structure is shown in Fig. 1. Note that in Fig. 1 all possible lithium sites are shown as occupied for presentation purposes. The distribution of lithium ions between these sites is discussed in what follows. In $Li_4Ti_5O_{12}$, the octahedral 16*d* sites are randomly occupied by lithium and titanium, the tetra-

* Corresponding author at: Pacific Northwest National Laboratory, Biological Monitoring and Modeling, 3335 Q Avenue, MSIN K8-98, Richland, WA 99352, USA. Tel.: +1 509 371 6544; fax: +1 509 371 6546.
E-mail addresses: Vijayakumar.murugesan@pnl.gov (M. Vijayakumar), Jianzhi.Hu@pnl.gov (J. Hu).

0378-7753/$ – see front matter © 2010 Elsevier B.V. All rights reserved.
doi:10.1016/j.jpowsour.2010.09.060

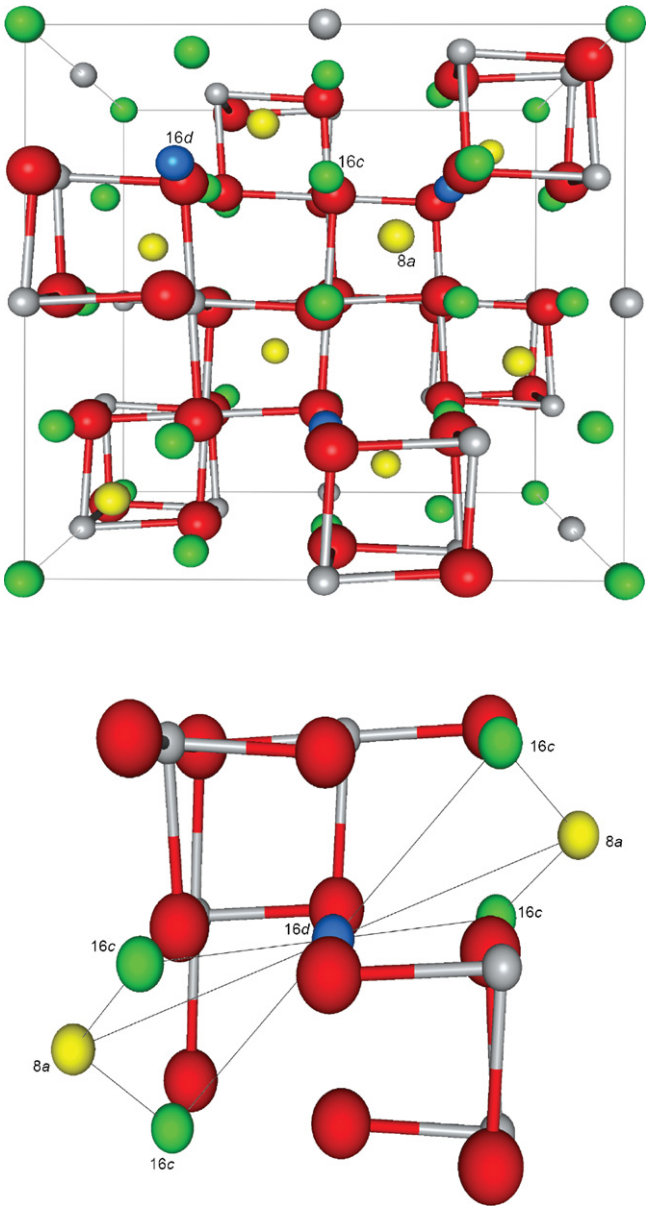

Fig. 1. Top figure: crystal structure of $Li_4Ti_5O_{12}$ showing the three lithium sites: tetrahedral 8*a* (white), octahedral 16*c* (grey) and octahedral 16*d* (black). Titanium and oxygen atoms are shown as small dark grey and large light grey balls, respectively. All three sites are shown as occupied for presentation purposes. The occupancy of these sites will vary with Li content and temperature, as discussed in the text. Bottom figure: inter-atomic distances between 16*d*–16*c* (2.95 Å), 16*c*–8*a* (1.81 Å), and 8*a*–16*d* (3.46 Å) site pairs based on the structure reported by Kataoka et al. [23].

hedral 8*a* sites are occupied by lithium only and the 16*c* sites are vacant. Upon lithium insertion, the lithium ions move from the 8*a* to the 16*c* sites and, at a composition of $Li_7Ti_5O_{12}$, a rocksalt structure is formed whereby all 16*c* sites are occupied and all 8*a* sites are empty. Lithium insertion is therefore proposed to be limited by the number of available 16*c* sites. However, as already mentioned, higher lithium contents have been reported [10–12], whereby the 8*a* sites begin to fill once all 16*c* sites are occupied. Such an insertion behavior suggests that lithium insertion is limited by the number of tetravalent titanium ions rather than by the number of available octahedral sites.

$Li_4Ti_5O_{12}$ shows a remarkably flat charge and discharge potential of approximately 1.55 V [4–6]. Therefore, lithium insertion was suggested to follow a two-phase reaction based on the observed flat charge potential, whereby $Li_4Ti_5O_{12}$ and $Li_7Ti_5O_{12}$ domains coexist and the reaction front advances in the material as the reaction proceeds [5]. Scharner et al. [24] provided evidence of a two-phase transformation upon lithium insertion based on X-ray diffraction (XRD) data and analysis of high-angle reflections, which allowed for the determination of a linear variation of the proportion of the two phases with increasing lithium content. Interestingly, Wagemaker et al. have shown using neutron and X-ray diffraction that in the absence of an applied potential the two-phase structure relaxes to a solid solution [25]. This phenomenon was previously alluded to by Ronci et al. [26] on the basis of changes in lattice parameters determined from in-situ synchrotron radiation XRD. A later study by Wagemaker et al. revealed 8*a* ($Li_4Ti_5O_{12}$) and 16*c* ($Li_7Ti_5O_{12}$) domain sizes on the order of a few nanometers [27].

$Li_4Ti_5O_{12}$ also shows interesting properties at high temperatures [28,29]. For example, $Li_4Ti_5O_{12}$ undergoes a nearly six-order-of-magnitude increase in conductivity ($\sim 10^{-3}$ S cm^{-1}) at high temperatures (>600 K) compared to the low conductivity ($\sim 10^{-8}$ S cm^{-1}) observed at room temperature [29]. This enormous increase in conductivity has been interpreted as the formation of a disordered state at high temperatures, whereby lithium randomly distributes between the 8*a* and 16*c* sites. The displacement of lithium ions from the 8*a* to the 16*c* sites with temperature and the formation of a disordered state have been inferred on the basis of changes in the intensities of infrared and Raman modes with temperature [28,29] but has not yet been confirmed with other experimental probes.

To provide further insights into the changes in lithium site distribution and diffusion behavior in $Li_4Ti_5O_{12}$ with temperature, we have carried out ^{6}Li magic angle spinning (MAS) nuclear magnetic resonance (NMR) measurements in combination with molecular dynamics (MD) simulations. $Li_4Ti_5O_{12}$ has previously been studied with ^{7}Li NMR; however, the data in these studies were acquired at low magnetic fields ($\leq$11.7 T), and hence might have suffered from poor spectral resolution [30,31]. Furthermore, these measurements were carried out at temperatures of at most 500 K and were therefore not able to probe the disordered phase and related increase in conductivity above 600 K. In the present work, variable-temperature ^{6}Li MAS NMR measurements were performed up to 700 K and under high magnetic field (21.1 T) to explore the lithium local structure and diffusion in $Li_4Ti_5O_{12}$ at high temperatures. Although NMR can offer a conspicuous view of the diffusion properties of complex materials, interpretation of NMR data is theoretically complex and thus often relies on complementary information from computational models to elucidate the ion distribution and dynamics. For example, in a recent study [32], results obtained from MD simulations helped assign the three resonance peaks obtained in NMR measurements of Li_2TiO_3. In this work, experimental NMR data is combined with results from molecular dynamics simulations to determine the lithium distribution and diffusion in $Li_4Ti_5O_{12}$ at high temperatures.

2. Experimental

The spinel type $Li_4Ti_5O_{12}$ material is prepared by modified pechini type sol–gel method using non-alkoxide materials similar to previous report [33]. To prepare 1 g of $Li_4Ti_5O_{12}$, 0.39 g of Ti metal powder was dissolved in an aqueous solution containing 20 mL of H_2O_2 (30%) and 5 mL of ammonia (35%) in an ice bath. This yielded a yellowish transparent titanium peroxo solution. Citric acid (15 g) was then added in excess to the titanium peroxo solution to form a metal chelate. High-purity Li_2CO_3 (0.246 g) was dissolved in denaturated ethyl alcohol. This solution was then added to the titanium peroxo solution and stirred well to ensure a homogeneous distribution. Ethylene glycol (20 g) was then added

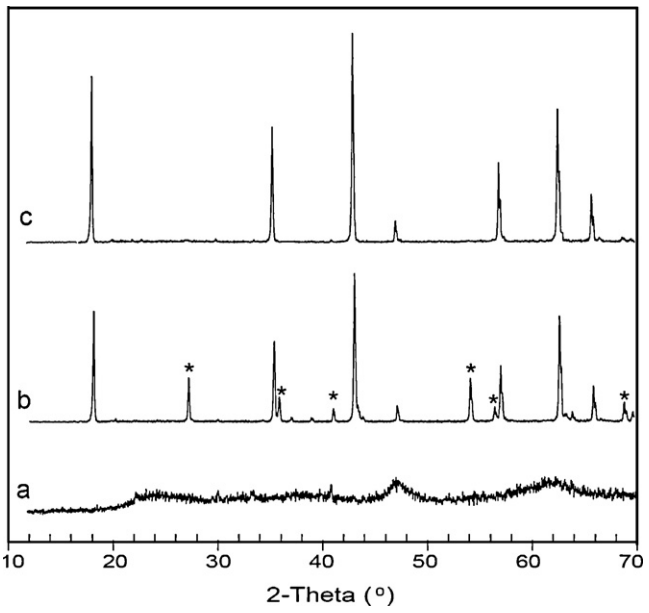

Fig. 2. XRD patterns of powder precursor samples heat-treated at different temperatures (a) 600 °C for 2 h, (b) 700 °C for 2 h, (c) 850 °C for 2 h. The spinel $Li_4Ti_5O_{12}$ diffraction lines are matched with JCPDS data (# 049-0207) and the rutile TiO_2 impurity phase indicated by the asterisk (*) are identified using JCPDS data (#021-1276).

to the above solution, which became reddish in color. The temperature was then increased to 150 °C for polymerization, which yields chemically stable black polymer precursor. Therefore, pyrolysis of the polymer was performed at 350 °C that yielded a black powder precursor. This final powder precursor was subjected to calcinations in open air for 2 h at temperatures between 600 and 850 °C. The resulting product from this sol–gel method was analyzed by X-ray powder diffractometry using a Philips Xpert X-ray diffractometer using CuKα radiation at $\lambda \sim 1.54$ Å. Fig. 2 shows the XRD pattern of the precursor after heat-treatment at different temperatures. The powder precursor, when heat-treated below 600 °C, is amorphous in nature. Its gray color indicates the presence of residual carbon. When heat-treated at 700 °C the powder appears white in color, which suggests the complete burnout of residual carbon from the precursor powders. The formation of the crystalline spinel phase (JCPDS# 049-0207) along with rutile (JCPDS#021-1276) was observed in the XRD patterns (see Fig. 2) for samples heat-treated at 700 °C. The highly crystalline and pure spinel phase has been identified for the samples heat-treated at 850 °C for 2 h. The crucial step adopted in our present study was to prepare a highly water-soluble starting precursor to avoid the use of alkoxides reported in previous literatures [17,18,34] which are not stable in open air. This was achieved by dissolving Ti metal in a solution of hydrogen peroxide and ammonia, as previously reported [35] which yield an air-stable and water-soluble peroxo–citrato–titanium complex as titanium source for sol–gel chemistry. Additionally, the relatively low temperature and the short time used in this synthesis minimize the lithium loss, as it is generally observed in the high-temperature heat treatments in other synthesis procedures [6,19]. Therefore, the modified sol–gel method used in this study offers an inexpensive and convenient aqueous synthesis approach that is scalable to meet the need of large scale commercial applications.

^{6}Li NMR measurements were performed on a Varian 900 Inova magnet ($B_0 = 21.1$ T and ^{6}Li Larmor frequency of 132.56 MHz) with magic angle spinning (MAS) at 7 kHz using 5 mm zirconia rotors and a home-made high-temperature MAS probe. The ^{6}Li spectra are recorded with single pulse measurements and the necessary recycle delay (d_1) was identified using array of d_1 varying from 1 to 700 s at each temperature. For the temperature range of our study, 500 s recycle delay was sufficient to acquire quantitative spectra at all temperatures. Chemical shifts were externally referenced to a 1 M LiCl solution ($\delta_{iso} = 0$ ppm). The estimated uncertainties in chemical shifts, determined through calibration using the same reference sample, were 0.1 ppm. Accurate chemical shifts and integral intensities of different contributions in each spectrum were obtained from fitting the line shapes of the resonance lines with a mix of Gaussian and Lorentzian line-shapes using the DMFIT program [36]. All the ^{6}Li NMR measurements were carried out on powder $Li_4Ti_5O_{12}$ sample without any ^{6}Li isotope enrichment.

3. Computational methods

3.1. Potential model

The calculations reported in this work are based on the Born model of solids [37], in which the atoms of a system are represented as point-charge particles that interact via long-range Coulombic forces and short-range interactions. The latter are described by parameterized functions and represent the repulsion between electron-charge clouds and the van der Waals attraction forces. In this work, the short-range interactions are described using a Buckingham potential and therefore the pair-wise interaction energy takes the following form:

$$U_{ij} = \frac{1}{4\pi\varepsilon_0}\frac{q_i q_j}{r_{ij}} + A_{ij}\exp\left(-\frac{r_{ij}}{\rho_{ij}}\right) - \frac{C_{ij}}{r_{ij}^6} \quad (1)$$

where the first term is the electrostatic potential energy and the second and third terms represent the electron-charge cloud repulsion and van der Waals attraction energies, respectively. The parameters (q, A, ρ, and C) used in this study for titanium and oxygen ions are those optimized by Matsui and Akaogi (MA) [38] for the TiO_2 polymorphs rutile, anatase, brookite, and TiO_2–II. The potential parameters used to describe lithium ions were determined by fitting the potential parameters for Li to the lattice parameters, lattice constants, and bulk modulus of Li_2O while keeping the MA potential parameters constant. The lithium partial charge was determined from the Li_2O stoichiometry while keeping the oxygen partial charge from the MA model constant (i.e., $q_{Li} = -q_O/2 = +0.549$ e). Details of the derivation of the Li parameters are provided in Supplemental information. In addition, our model accounts for the polarizability of oxygen ions via a shell model first introduced by Dick and Overhauser [39]. In the shell model, a polarizable ion is composed of two particles, a core and a shell, which share the ion's charge and are linked by a harmonic spring, k:

$$U_{c-s} = k \times r_{c-s}^2 \quad (2)$$

where r_{c-s} is the core–shell separation distance. The derivation of the shell model version of the MA potential is described in a previous publication [40]. This shell model has proved to be a reliable and transferable potential model. For example, it gives an excellent description of the crystal structure of several TiO_2 polymorphs and reproduces lattice distortions, obtained from density functional theory calculations, due to the introduction of hole and electron polarons in rutile and anatase crystal lattices [40]. In addition, the potential model yielded excellent agreement with the experimental crystal structure of Li_2TiO_3 and helped provide an explanation for the presence of a NMR peak with a chemical shift corresponding to a lithium tetrahedral site whereas the pure crystal structure only contains lithium ions in octahedral coordination [32]. All the potential parameters used in this work are summarized in Table 1.

The ability of the potential model for simulating $Li_4Ti_5O_{12}$ was evaluated by comparing the calculated and experimental lattice parameters. A 200-ps NPT molecular dynamics simulation at 300 K with the computer program DL_POLY [41] yielded $a = 8.443$ Å. X-

Table 1
Potential parameters used in this work. The oxygen core–shell spring constant, k, is set to 44.3 eV Å^{-2}.

Core and Shell charges[a]		
Species	Core (e)	Shell (e)
Ti^{4+}	2.196	–
Ti^{3+}	1.647	–
Li^{+}	0.549	–
O^{2-}	0.500	−1.598

Buckingham potential parameters[b]			
Ion pair (ij)	A_{ij} (eV)	ρ_{ij} (Å)	C_{ij} (eV Å^6)
Li–Li	38533.955	0.100	0.00
Ti–Li	33089.570	0.127	0.00
Ti–Ti	31120.528	0.154	5.25
Ti–O	16957.710	0.194	12.59
Li–O	15465.549	0.167	0.00
O–O	11782.884	0.234	30.22

[a] Core–shell interaction potential form: $V = k \times r_{c-s}^2$.
[b] Buckingham potential form: $V_{ij} = A_{ij} \times \exp(-r_{ij}/\rho_{ij}) - C_{ij} r_{ij}^{-6}$.

ray diffraction data of Deschanvres et al. [22] and Kataoka et al. [42] gave a = 8.357 Å and a = 8.352 Å, respectively. Wagemaker et al. [25] reported a value of the lattice parameter of 8.3595 Å from neutron diffraction data. The calculated lattice parameter is in good agreement with experimental data with an error of at most 1.1%. The potential model predicts a linear decrease in a with increasing Li content for $0 \le x \le 3$ in $Li_{4+x}Ti_5O_{12}$ in agreement with experimental data [25]. For $Li_7Ti_5O_{12}$, the molecular dynamics simulations predict a = 8.411 Å or a reduction of 0.4%, which is larger than that observed by Wagemaker et al. [25] (just under 0.1%) but of the same order of magnitude and similar (0.7%) to that calculated by Zhong et al. [12] using planewave density functional theory.

3.2. Molecular dynamics simulations

MD simulations were carried out with the computer program DL_POLY [41] at zero-applied pressure. Equilibration runs were initially performed in the NPT ensemble (constant number of particles, constant pressure, and constant temperature), whereby both the cell shape and size were able to vary, for 10 ps to obtain the average cell dimensions. Production runs were then carried out in the NVT ensemble (constant number of particles, constant volume, and constant temperature) for 10 ns with the cell dimensions fixed to the average values obtained in the equilibration runs. This was done to facilitate the mean square displacement analysis. In these simulations, the temperature and pressure were kept constant by use of the Nosé–Hoover thermostat [43] and the Hoover barostat [44], respectively. The electrostatic forces were calculated by means of the Ewald summation method [45]. A 9 Å cutoff was used for the short-range interactions and the real part of the Ewald sum. The Verlet leapfrog integration algorithm was used to integrate the equations of motion with a time step of 0.2 fs. The shells were given a mass of 0.2 a.u. and their motion treated as that of the cores following the adiabatic shell model first introduced by Mitchell and Fincham [46].

4. Results and discussion

4.1. High-temperature ^{6}Li MAS NMR

Fig. 3 shows the temperature dependence of ^{6}Li MAS NMR spectra of $Li_4Ti_5O_{12}$ acquired at a magnetic field of 21.1 T using a sample spinning speed of 7 kHz. At 295 K (bottom spectrum in Fig. 3), the $Li_4Ti_5O_{12}$ sample shows three overlapping resonances at 0.65, 0.17, and −0.45 ppm indicating three different crystallographic positions for lithium in $Li_4Ti_5O_{12}$, which agrees with single-crystal data [23,42]. Fig. 1 shows the crystal structure of $Li_4Ti_5O_{12}$ as reported by Kataoka et al. [23,42] with all possible lithium sites occupied. As previously explained, $Li_4Ti_5O_{12}$ has two octahedral and one tetrahedral lithium positions, which are labeled, in Wyckoff's notation, 16*c*, 16*d*, and 8*a*, respectively. The ^{6}Li NMR peak assignments were made based on previous reports of lithium insertion in titanium oxide materials [47–50] and ^{6}Li chemical shift correlation data [51]. According to ^{6}Li chemical shift correlation data [51], the nature of the lithium coordination environment is the main driving force for the observed chemical shift. For example, the chemical shift (with respect to 1 M aqueous LiCl solution) of lithium in tetrahedral coordination is expected around 1 ppm towards higher frequencies (positive shift) whereas that of lithium in octahedral coordination is expected around −1 ppm (negative shift). Following this chemical shift correlation data, the tetrahedral position (8*a*) can be assigned to the ^{6}Li resonance at 0.65 ppm whereas the two octahedral lithium positions, i.e., 16*d* and 16*c*, can be assigned to the ^{6}Li resonances observed at 0.17 and −0.45 ppm, respectively, based on previous reports [47–50]. It is interesting to note that lithium in the two octahedral positions shows distinct ^{6}Li chemical shifts. The difference in chemical shift between these two octahedral positions can be explained by the fact that, although both 16*c* and 16*d* lithium sites are octahedrally coordinated by oxygen, they have different next-nearest neighbors. The Li(16*c*)O_6 octahedron is in a corner-sharing configuration with TiO_6 octahedra, whereas Li(16*d*)O_6 octahedra are in corner-sharing configurations with vacant and Li(16*c*)O_6 octahedra. Such a difference in the nature of the lithium next-nearest neighbors is likely to be responsible for the observed difference in chemical shifts between the 16*c* and 16*d* sites. Indeed, the significant effect of next-nearest neighbors

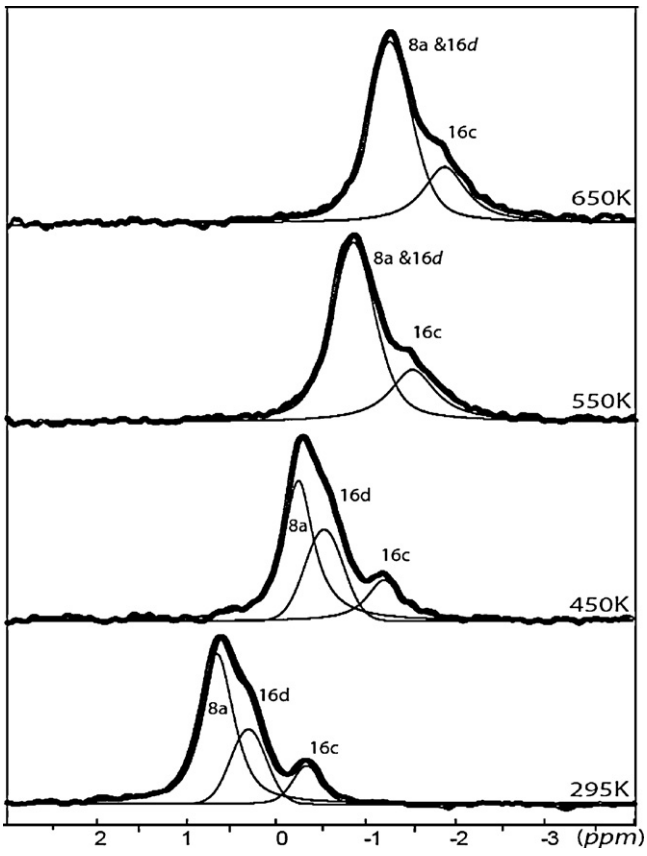

Fig. 3. (a) ^{6}Li MAS NMR spectra measured with a 21.1 T magnetic field and spinning speed of 7 kHz for $Li_4Ti_5O_{12}$. The peaks are labeled with Wyckoff's notation for different lithium positions in $Li_4Ti_5O_{12}$.

has been documented previously, for example, for ^{23}Na and ^{93}Nb chemical shifts [52,53].

Additionally, of all the NMR spectra collected in this study, that obtained at 295 K offers the best resolution of the three resonance peaks. The integral intensities determined from this spectrum are $62 \pm 3\%$, $24 \pm 3\%$, and $14 \pm 2\%$ for the resonances positioned at 0.65, 0.17, and −0.45 ppm, respectively. This observation provides further support for the assignment presented above as 24% corresponds within uncertainty to the expected proportion of Li ions in 16*d* sites, whereas inversing the assignment of the two octahedral sites would result in 12% of the Li ions in 16*d* sites, which, in turn, would imply an unrealistically large number of vacancies in 16*d* sites. Finally, as explained in detail below, the integral intensity of the resonance assigned to the 16*c* site increases significantly with temperature. This observation is consistent with our assignment given that inversing the assignment of the two octahedral sites would signify that vacancies at 16*d* sites are progressively filled by lithium ions as the temperature increases. However, this phenomenon would go directly against the observations of Leonidov et al. [54], who reported the formation of vacancies at 16*d* sites with increasing temperature.

Having assigned all three peaks, the variable-temperature ^{6}Li MAS NMR spectra can offer further information on the possible lithium diffusion behavior in $Li_4Ti_5O_{12}$ by studying the temperature dependence of the peak positions. Fig. 4a shows the temperature dependence of the ^{6}Li chemical shift of all three lithium resonances. Two general phenomena should be noted to interpret the NMR data. Firstly, thermal expansion of a material can lead to monotonic changes in chemical shift due to changes in bond lengths and bond angles [55]. Secondly, an increasing extent of lithium hopping between two different sites leads to the coalescence of the corresponding ^{6}Li resonance peaks. The main characteristic feature of coalescence is the change in isotropic chemical shift observed when two peaks, representing two different chemical sites, move toward each other. After such coalescence, the coalesced peak width will narrow with increasing temperature due to motional narrowing effects [56].

As can be seen from Fig. 4a, all three peaks show shifts towards lower shielding (or decreased ppm) with increasing temperature. Therefore, this general trend can be attributed to the thermal expansion of the material with temperature. Below 525 K, the 8*a* peak shows significant change in its isotropic chemical shift and moves towards the 16*d* peak and above 525 K the 8*a* and 16*d* peaks become inseparable. However, this may not represent the coalescence of the 8*a* and 16*d* resonances due to the fact that the coalescence should be followed by narrowing of the coalesced peak, but all the peaks show an increase in line width over the whole temperature range. These observations lead us to conclude that the broad peak above 525 K is not the result of the coalescence of the 8*a* and 16*d* peaks, but instead is due to the broadening of the 8*a* and 16*d* peaks to the extent that they strongly overlap and thus cannot be clearly resolved. In other words, there is no significant lithium exchange between the 8*a* and 16*d* sites which could lead to the coalescence of these signals. This conclusion is supported by our molecular simulations, which will be presented later, as well as by previous studies reported by other researchers [50,54,57], which indicate that lithium ions in 16*d* sites are not participating in any exchange processes at these temperatures.

Deconvolution of the 8*a* and 16*d* resonances above 525 K, would result in unacceptable uncertainties; therefore, we decided to fit the broad peak with a single resonance. Above 525 K, the combined 8*a*/16*d* peak and the 16*c* peak move towards higher shielding (i.e., towards negative ppm). At the same time, both the 8*a*/16*d* and 16*c* peaks show an increase in line width with temperature, an indication of possible coalescence. However, the strong overlap

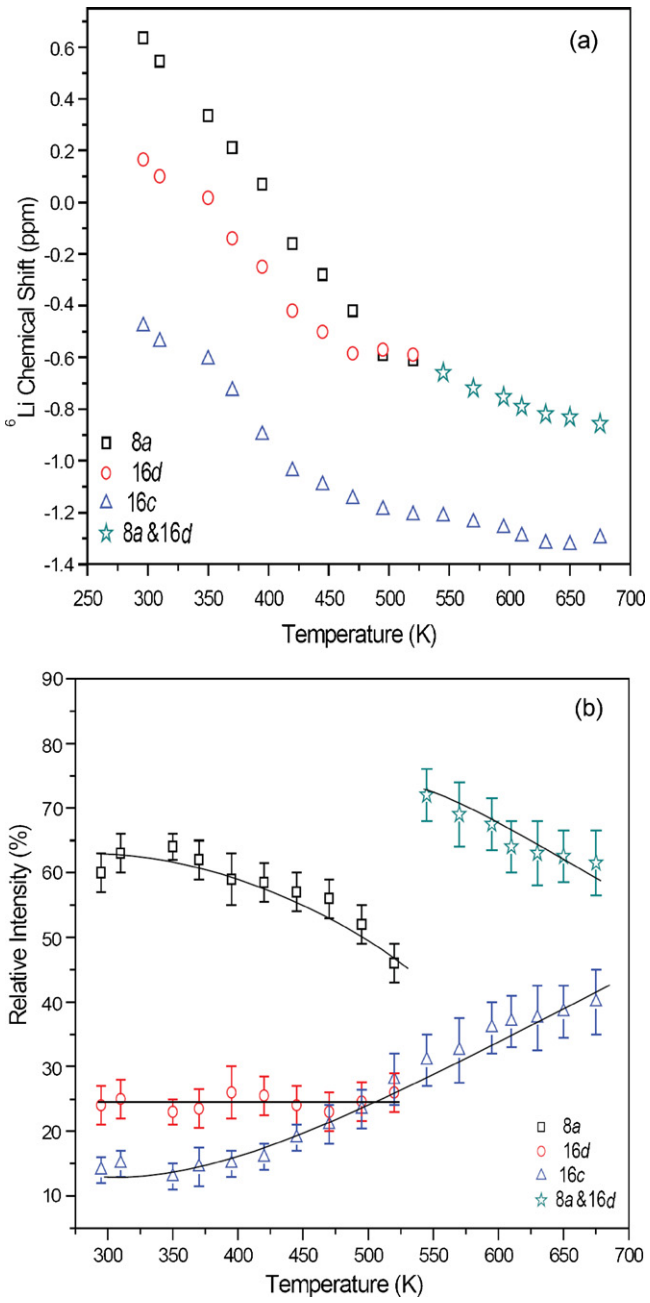

Fig. 4. Temperature dependence of deconvoluted parameters (a) isotropic ^{6}Li chemical shift and (b) integral intensity from variable temperature ^{6}Li MAS NMR spectra measured at 21.1 T with spinning frequency of 10 kHz for $Li_4Ti_5O_{12}$ (lines are to guide the eye). The peaks 8*a* and 16*d* are inseparable above 525 K, hence the star symbol represents the combination of both 8*a* and 16*d* peaks.

between the 8*a* and 16*d* resonances prevents us from accurately determining the position of the 8*a* maximum. As a result, we cannot resolve any potential coalescence of the 8*a* and 16*c* resonances; however, the data obtained above 525 K do not rule out coalescence either. Lithium hopping between 8*a* and 16*c* sites is expected to take place based on our molecular dynamics simulations as well as previous studies [50,54,57]. Therefore, in order to explore the lithium exchange between the 8*a* and 16*c* sites further, we analyzed the temperature dependence of the integral intensity of the ^{6}Li resonances.

Fig. 4b shows the temperature dependence of the ^{6}Li integral intensity of all three lithium resonances. The integral intensity of the 16*c* peak increases from 12% at 300 K to about 40% at 675 K

at the expense of the 8*a* peak, which decreases drastically with increasing temperature. This result clearly indicates a progressive redistribution of the lithium ions from the 8*a* site to the 16*c* site as the temperature increases. Such a lithium migration should ultimately lead to the coalescence of the respective ^{6}Li peaks. Indeed, the complete migration of lithium from 8*a* to 16*c* sites would lead to a defective NaCl-type structure (space group $Fm\bar{3}m$), whereby lithium ions and cation vacancies distribute over the 16*c* sites.

The relocation of lithium from the 8*a* to the 16*c* site with increasing temperature could have a detrimental effect on the electrochemical performance of $Li_4Ti_5O_{12}$. It has been reported that, as a result of electrochemical lithium insertion, lithium ions move from the 8*a* to 16*c* sites [6,58] and consequently, electrode performance is dependent on the number of available 16*c* sites in the structure. The present high-temperature NMR results show that a similar relocation of lithium ions from 8*a* to 16*c* sites is caused by increasing temperature. This relocation could adversely affect the number of free 16*c* sites available for electrochemical lithium insertion and thus may lead to poor electrode performance of $Li_4Ti_5O_{12}$. However, it is worthwhile to mention that this effect becomes significant at temperatures well above the normal operating temperature of lithium batteries.

Further, it is interesting to note that there is no significant change in the integral intensity of the 16*d* peak with increasing temperature (up to 525 K), which suggests that there is no net lithium migration from 16*d* positions to other sites in this temperature range. Such a lithium migration from 16*d* to 16*c* was observed above 800 K by Leonidov et al. [29] leading to a second phase transformation and the formation of an ordered NaCl-type structure. Unfortunately, due to technical difficulties in building a very high temperature NMR probe (>700 K), we were not able to verify the occurrence of this second phase transformation (where all lithium ions in 16*d* sites move to 16*c* sites). Nonetheless, the present NMR results suggest that the completion of a phase transformation of $Li_4Ti_5O_{12}$ from a spinel to a defective NaCl-type structure should occur at temperatures above 700 K. This result is consistent with the previous high-temperature spectroscopic studies [28,29] of $Li_4Ti_5O_{12}$ discussed in Section 1.

To provide further evidence for the lithium diffusion behavior determined on the basis of ^{6}Li MAS NMR, we carried out two-dimensional (2D) ^{6}Li exchange spectroscopy (EXSY) [59]. Fig. 5 shows the ^{6}Li 2D EXSY spectra obtained at 350 and 570 K with a mixing time (τ_{mix}) of 1 s and a spinning speed of 7 kHz under a magnetic field of 21.1 T. In 2D EXSY spectra, if the exchange between any two sites is slow relative to the selected mixing time then peaks appear only on the diagonal position. On the other hand, if the timescale for exchange is faster than τ_{mix}, cross peaks appear at the co-ordinates of the corresponding diagonal peaks [59].

The ^{6}Li 2D EXSY spectrum obtained at 350 K (see Fig. 5a) clearly shows the absence of any cross peaks. The detection of cross peaks corresponding to exchange between the 8*a* and 16*c* resonances could have been made difficult by the lithium diffusion pathways operating in this material at this temperature. At 350 K, more than 60% of the lithium ions reside in 8*a* sites whereas the 16*c* sites only account for approximately 10% of the lithium ions. Therefore, most of the lithium diffusion involves lithium ions diffusing from 8*a* to 8*a* sites. However, considering the crystal structure of $Li_4Ti_5O_{12}$ (see Fig. 1), lithium hopping between two 8*a* sites has to take places via a 16*c* site. We propose that, given the lithium partition between the 8*a* and 16*c* sites, lithium occupancy of the 16*c* site is expected to be transient and thus would not be detected in the 2D EXSY experiments. Indeed, in the $Li_4Ti_5O_{12}$ structure, a 16*c* site has four nearest-neighbor 8*a* sites at 1.84 Å. In addition, based on the lithium partition between the 8*a* and 16*c* sites derived from ^{6}Li MAS NMR, a lithium ion in a 16c site has, on average, 3.4 occupied nearest-neighbor 8*a* sites at 350 K. Such a close proximity between lithium ions in 8*a* and 16*c* sites makes the 16*c* site energetically costlier due to Li–Li repulsive electrostatic interactions. Such a diffusion behavior has already been proposed by Wagemaker et al. [50], who concluded, based on the results of 1D and 2D ^{7}Li MAS NMR, that lithium ions will spend negligible time in 16*c* sites while diffusing between 8*a* sites. Additionally, although our experiments do not

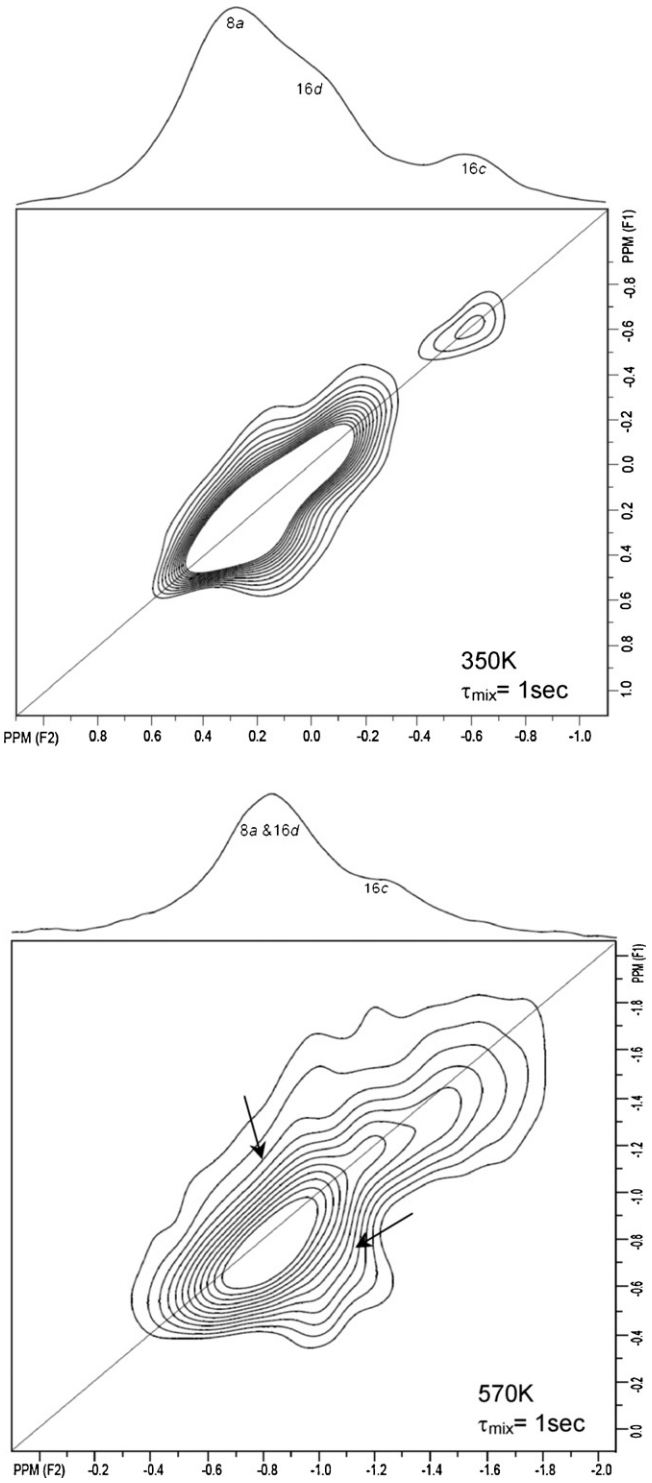

Fig. 5. Two dimensional (2D) ^{6}Li exchange spectroscopy (EXSY) spectra of $Li_4Ti_5O_{12}$ measured with a 21.1 T magnetic field and spinning speed of 7 kHz at 350 K (a) and 570 K (b). The mixing time (τ_{mix}) is kept at 1 s to ensure the detecting of cross peaks due to very slow jump rates (in the order few Hz). The single pulse ^{6}Li MAS NMR spectra at respective temperature are plotted on the top of the 2D spectra for clear spectral assignments. The arrows indicate the expected position of cross peaks.

provide further direct evidence, it is worthwhile to mention that our results are consistent with the nano-domain model proposed by Wagemaker et al. [50], in which lithium distributes between separate 8*a*- and 16*c*-rich nano-domains.

With increasing temperature, the proportion of lithium ions at 8*a* sites decreases considerably (see Fig. 4b), thereby increasing the probability of jumps between 8*a* and 16*c* sites. Any such jumps between 8*a* and 16*c* sites can be detected in 2D EXSY measurements. Fig. 5b shows the 2D EXSY spectrum measured at 575 K. The arrows indicate the expected positions of the cross peaks that would arise from any diffusion between 8*a* and 16*c* sites. Unfortunately, identification of the cross peaks is difficult due to the severe overlap between the ^{6}Li resonances. As a result, the low spectral resolution obtained at high temperatures prevented us from clearly identifying the cross peaks and calculating the lithium jump rate between 8*a* and 16*c* sites. However, it should be noted that all spectra were measured at magnetic field of 21.1 T, which is higher than any magnetic field used in studies of lithium diffusion in this material published to date. Therefore, although not always sufficient for determining all the properties of interest with high accuracy, we note that it is the very high resolution of the NMR measurements presented in this work which makes this study possible.

Based on our conclusions regarding lithium migration, we can attempt to explain the considerable increase in the conductivity of $Li_4Ti_5O_{12}$ at high temperatures reported in the literature [29]. The integral intensity of the 8*a* peak decreases from 62% at room temperature to 48% at 525 K (see Fig. 4b). Such migration leads to a high concentration of vacancies at 8*a* sites thereby facilitating lithium diffusion through $16c \rightarrow 8a \rightarrow 16c$ pathways. The 16*d* octahedral site shows no significant lithium diffusion in our NMR spectra, therefore the substantial increase in the conductivity reported in $Li_4Ti_5O_{12}$ at high temperatures [29] is caused by the increased probability of lithium diffusion between octahedral 16*c* sites through nearby vacant 8*a* sites. In order to cross-examine the lithium migration and diffusion characteristics observed by NMR at high temperatures, we carried out an extensive molecular dynamics study of lithium diffusion in this material.

4.2. Lithium distribution between crystallographic sites

In this section, we present results obtained from molecular dynamics simulations of $Li_4Ti_5O_{12}$ carried out at a range of temperatures in order to complement the NMR data discussed above. In addition, we extended our study to consider higher lithium contents, i.e., $Li_{4+x}Ti_5O_{12}$ with $0 \leq x \leq 3$. This allows for a direct comparison with published experimental data of Li distribution between crystallographic sites and thus constitutes an additional evaluation of the potential model. Moreover, as the lithium content can be easily varied in the molecular simulations, it allows us to investigate how the conclusions drawn from the study of $Li_4Ti_5O_{12}$ extend to compounds with higher lithium contents. Therefore, four different lithium contents were considered, namely, $Li_{4+x}Ti_5O_{12}$ with x equals to 0, 1, 2, or 3. For each value of x, a series of MD simulations was carried out whereby the temperature was varied from 300 to 700 K with 100 K intervals to reproduce the temperature range used for the NMR measurements. In each simulation, The Ti^{3+}/Ti^{4+} distribution in the supercell was determined randomly and was kept fixed during the MD simulation. For each simulation, the lithium distribution between the three crystallographic positions (Fig. 1) was determined as follows: (a) the average titanium positions were computed using the entire run; (b) the lithium crystallographic positions were calculated from the average titanium positions and the known crystal symmetry; (c) radial distribution functions (RDFs) were constructed using the instantaneous lithium positions relative to each of the three crystallographic sites; and (d) an integration of each RDF plot to its first minimum yielded the occupancy of the three sites. Table 2 shows the lithium distributions at all temperatures and all Li contents and Fig. 6 compares the lithium distribution at 300 K with the experimental data of Scharner et al. [24], Wagemaker et al. [25], and Kataoka et al. [42]. The MD simulations predict a full occupancy of the 16*d* sites based on the stoichiometry at all temperatures in agreement with the experimental data of Wagemaker et al. and Kataoka et al. as well as our NMR data. The potential model also shows a Li distribution between the 8*a* and 16*c* sites in excellent agreement, for all lithium contents, with the room temperature experimental data of Scharner et al. and Kataoka et al., with only a slight overestimation of the occupancy of the 8*a* site at higher Li contents. The data of Wagemaker et al. is shifted to higher Li contents but follow the same trend as the XRD and MD results.

Table 2
Population of each crystallographic site as a function of temperature and lithium content as determined from the molecular dynamics simulations.

Li content, x	300 K	400 K	500 K	600 K	700 K
8a					
0	74	74	74	73	73
1	50	49	49	49	49
2	30	29	28	28	28
3	13	12	12	11	12
16c					
0	1	1	3	4	4
1	31	31	31	32	32
2	54	54	56	56	57
3	73	74	74	75	75
16d					
0	25	25	24	24	23
1	20	20	20	20	20
2	17	17	17	17	17
3	14	14	14	14	14

Turning now to the temperature dependence, our MD simulations show an increase in the occupancy of the 16*c* site to the detriment of the 8*a* site with increasing temperature (Table 2). Although this trend is in agreement with the NMR data obtained in this work, it is not as pronounced as observed experimentally. As mentioned previously, Raman [29] and infrared [28] spectroscopy experiments also indicate the migration of lithium ions from the 8*a* to the 16*c* site with increasing temperature. To conclude, it is not clear why the lithium content dependence of the Li distribution is well reproduced whereas the temperature dependence is far too weak compared to experiment. This result might suggest that the

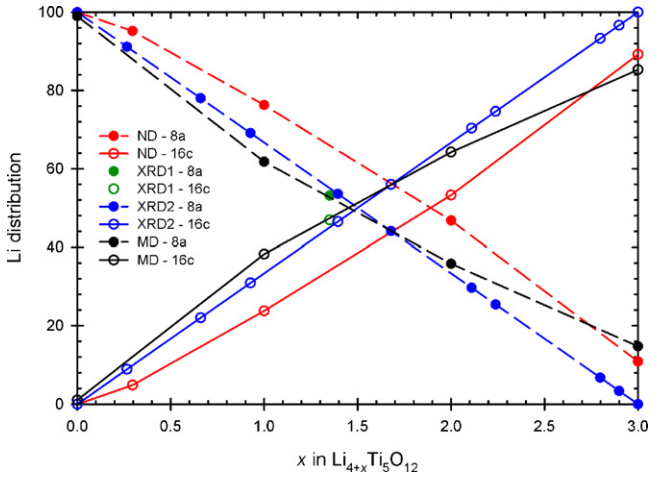

Fig. 6. Lithium distribution between the 8*a* and 16*c* sites as a function of Li content as obtained from molecular dynamics simulations (this work), neutron diffraction (ND [25]), and X-ray diffraction data (XRD1 – Kataoka et al. [42] and XRD2 – Scharner et al. [24]).

strength of the Li–Li repulsion relative to the Li–O potential is well reproduced by the potential model but that the Li–O interaction is too attractive with respect to the thermal energy.

4.3. Lithium diffusion between crystallographic sites

The same series of MD simulations was used to extract information about the rate and mechanism of lithium diffusion for each of the four lithium contents. As will be demonstrated in this subsection, the rates of exchange between the different crystallographic sites span a large range of timescales. Therefore, two approaches were used to determine the rates of lithium exchange as a function of temperature and thus extract activation energies to be compared with experimental data.

The first approach consists of calculating the population correlation function, $C(t)$, for lithium hopping between pairs of crystallographic sites. $C(t)$ is defined as [60]:

$$C(t) = \frac{\langle h_A(0)h_B(t)\rangle}{\langle h_A(0)\rangle} \quad (3)$$

where $h_i(x)$ is 1 if the lithium ion is in site i at time x and 0 otherwise. Correlation was followed for 20 ps and $C(t)$ was obtained by averaging the contribution of all lithium ions. As explained by Chandler [60], this correlation function approaches its asymptotic value exponentially:

$$C(t) \approx \langle h_B\rangle \left[1 - \exp\left(\frac{-t}{\tau_{rxn}}\right)\right] \quad (4)$$

where τ_{rxn} is the inverse of the sum of the forward (k_{AB}) and backward (k_{BA}) reaction rates. In addition, if τ_{rxn} is much larger than the molecular time scale (τ_{mol}), $C(t)$ is linear in the time regime $\tau_{mol} < t \ll \tau_{rxn}$ and its gradient is equal to k_{AB}.

The second approach consists of computing the residence time correlation function, $R(t)$:

$$\langle R(t)\rangle = \left\langle \frac{1}{N_0}\sum_{i=1}^{N_t}\theta_i(0)\theta_i(t)\right\rangle \quad (5)$$

where N_t is the number of lithium ions in the crystallographic site of interest at time t and $\theta_i(t)$ is the Heaviside function, which is 1 if the ith lithium ion is in the crystallographic site of interest at time t and 0 otherwise. The crystallographic sites were considered to extend to the first minima of the radial distribution functions described in the previous subsection. As it is usually done with such an analysis [61], a lithium ion was counted as having left its crystallographic site if it has done so for any continuous period of time of at least t^*. This is to allow for lithium ions that temporarily leave the crystallographic site and come back without visiting another site for a significant amount of time to be counted in the residence time. A value of 0.5 ps for t^* was employed in this work. The residence time and thus the exchange rate, k, can then be obtained by integration of $\langle R(t)\rangle$:

$$\frac{1}{k} = \tau = \int_0^\infty \langle R(t)\rangle\, dt \quad (6)$$

The first approach is appropriate when $\tau_{mol} \ll \tau_{rxn}$ whereas the second approach converges faster the faster the exchange rate.

The population correlation functions were calculated for lithium exchange between 8*a* and 16*d*, 16*d* and 16*c*, and 16*c* and 8*a*. These functions revealed that there are no direct exchanges between the 8*a* and 16*d* sites. Indeed, inspection of the crystal structure shows that the 16*c* site is closer to 16*d* than to 8*a* (see Fig. 1) and the population correlation function therefore confirms the expectation that the lithium ions hop first to 16*c* from 16*d*. As expected, the 16*d*–16*c* correlation function shows a linear behavior at all temperatures

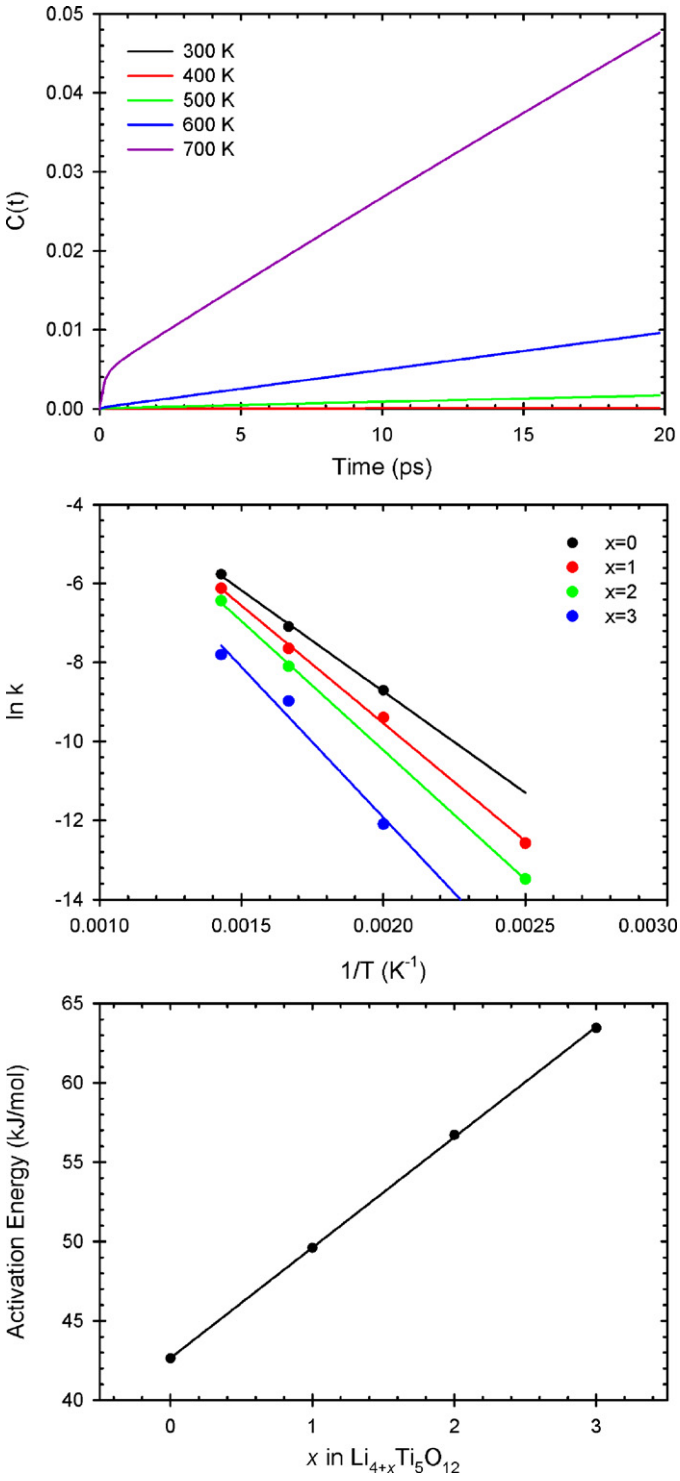

Fig. 7. Population correlation function for the 16*d*–16*c* Li exchange as a function of temperature (top); rate of Li exchange between the 16*d* and 16*c* sites as a function of temperature for each Li content (middle); activation energy for the 16*d*–16*c* Li exchange as a function of Li content (bottom).

(see Fig. 7 for an example), whereby the gradient of each straight line yields the forward rate constant. A plot of the logarithm of the rate constant as a function of the inverse temperature (Fig. 7) gives the activation energy for each Li content. Interestingly, Fig. 7 also shows that the activation energy for lithium hopping between the 16*d* and 16*c* sites is a linear function of the lithium content with activation energies from approximately 43 kJ mol^{-1} for $x = 0$ to 63 kJ mol^{-1} for $x = 3$.

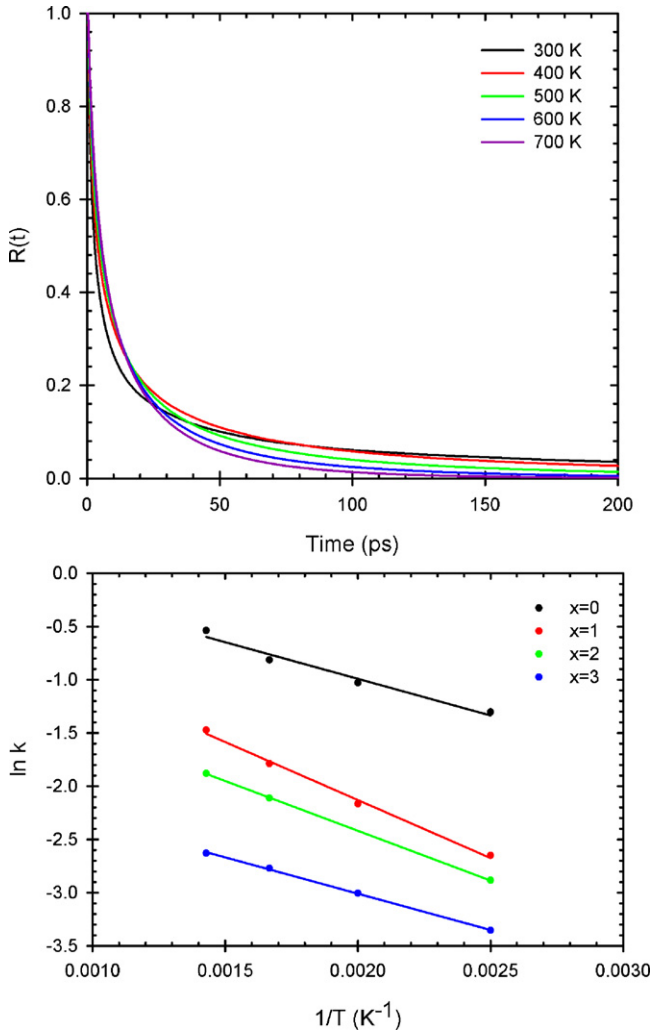

Fig. 8. Li residence time in the 16*c* site for $x = 3$ at all temperatures (top) and rate of exchange as a function of temperature for all Li contents (bottom).

The exchange between the 16*c* and 8*a* sites was fast with no distinct linear regime. Therefore, the lithium residence time in each of the 8*a* and 16*c* sites was calculated using the second approach. The residence time correlation function of lithium in the 16*c* site for $x = 3$ at all temperatures is shown in Fig. 8 as an example. The rate of exchange is then obtained from Eq. (6). The activation energies for hopping from both sites initially increase, reach a maximum and then decrease again with increasing Li content. However, the maximum activation energies are obtained at different Li contents. The calculated activation barriers are of the order of 5–10 kJ mol^{-1} and are therefore much lower than the activation energy values of approximately 30 kJ mol^{-1} derived by Wagemaker et al. [27] from NMR correlation times of lithium hopping on the 8*a* and 16*c* sublattices. The activation barriers obtained by Wagemaker et al. were for mixed 8*a*/16*c* occupation (i.e., $x = 0.3$, 1, and 2) and no lithium diffusion was observed for the structural end members, $x = 0$ and 3. This observation is consistent with the ultraslow Li diffusion reported by Wilkening et al. [30,31] for $x = 0$. In our molecular dynamics calculations, it is likely that a hop out of either site is often followed by a backward hop to the same site thus leading to no net lithium diffusion. To address this issue, we calculated the overall lithium diffusion coefficient as a function of temperature to extract mean activation energies for lithium diffusion whereby the lithium diffusion coefficients were obtained from the gradients of the mean square displacement functions. Table 3 shows the overall activation energies as a function of Li content. The activation energies obtained from the MSD functions are much higher than those computed from the residence time correlation functions, which confirm the hypothesis stated above. The activation energies for the mixed occupation values are lower than those obtained experimentally by Wagemaker et al. [27] (~30 kJ mol^{-1}) and Wilkening et al. [30] (~40 kJ mol^{-1}). In addition, the activation energies for the structural end members are much lower than those derived experimentally (70–90 kJ mol^{-1}) [31]. However, the weak dependence of the calculated activation energies on the Li content for the mixed occupation compositions agrees with the experimental observation of Wagemaker et al. [27].

Table 3
Activation energies (kJ mol^{-1}) for lithium hopping from the 8*a* and 16*c* sites in $Li_{4+x}Ti_5O_{12}$ as determined from residence time correlation functions and activation energies for overall lithium diffusion as obtained from mean square displacement functions.

Site	$Li_4Ti_5O_{12}$	$Li_5Ti_5O_{12}$	$Li_6Ti_5O_{12}$	$Li_7Ti_5O_{12}$
8*a*	4.2	7.0	9.3	8.5
16*c*	5.2	8.6	7.3	5.3
Overall	26.8	21.5	20.3	19.6

In conclusion, the molecular dynamics simulations show that the free energy barrier for lithium hopping between the 8*a* and 16*c* sites is much lower than that between the 16*d* and 16*c* sites and that therefore the onset of the first transfer should occur at a lower temperature. This is in agreement with the NMR findings and, although the motion of the Li ions in 16*d* positions was not observed in the NMR experiments, the work of Leonidov et al. [29] indicates that the 16*d* Li ions begin to move at temperatures higher that those probed in this work.

5. Conclusions

Highly crystalline $Li_4Ti_5O_{12}$ has been synthesized by a modified non-alkoxide-based sol–gel method, where the final calcination is performed at a lower temperature and for a shorter period of time than in previously reported sol–gel methods. This sol–gel synthesis method constitutes a simple and cost efficient preparation method suitable for bulk industrial preparations. High temperature ^{6}Li MAS NMR measurements of the synthesized $Li_4Ti_5O_{12}$ sample reveal the migration of lithium ions from the tetrahedral 8*a* sites to the octahedral 16*c* sites leading to a defective NaCl-type structure. This lithium relocation could restrict the number of free 16*c* sites available for external lithium insertion and may lead to poor electrode performance of $Li_4Ti_5O_{12}$. Due to this phase transformation, the operating temperature of any $Li_4Ti_5O_{12}$ based lithium battery should be kept below 500 K. Interestingly, the lithium ions in octahedral 16*d* sites show no significant diffusion process in the experimental temperature range. The change in lithium population observed between the 8*a* and 16*c* peaks also suggests lithium diffusion through $16c \rightarrow 8a \rightarrow 16c$ pathways, which is facilitated by the large number of vacancies formed at 8*a* sites. Therefore, the large increase in conductivity observed for $Li_4Ti_5O_{12}$ at high temperatures (>600 K) is mainly due to the high lithium diffusion between 16*c* sites through vacant 8*a* sites.

Our potential shell model gives a good structural description of the spinel oxides $Li_{4+x}Ti_5O_{12}$ ($0 \leq x \leq 3$) and an excellent agreement with the experimentally-derived Li distributions between the 8*a* and 16*c* sites as a function of Li content. However, the depth of the free energy minima of either or both of the 8*a* and 16*c* positions is probably too shallow, which leads to a higher Li diffusion and is also likely to be the cause of the smaller temperature dependence of the Li distribution between the 8*a* and 16*c* sites. Despite the discrepancies in the absolute values of the activation energy for lithium diffusion, important information emerged from the molec-

ular dynamics simulations concerning the relative dynamics of exchange between the different lithium sites in support of our high temperature ^{6}Li MAS NMR data. At first, the exchange between the 8*a* and 16*c* sites is relatively faster whereas that between the 16*d* and 16*c* sites is slow and that there is no direct exchange between the 16*d* and 8*a* sites. Additionally, the occupancy of the 16*d* sites remains at nearly the stoichiometric level at all temperatures studied as it is found in the NMR analysis of the relative peak intensities. Finally, this study demonstrates the importance and effectiveness of combining information obtained from NMR measurements and MD simulations to draw a comprehensive picture of the microscopic lithium diffusion processes in electrode materials.

Acknowledgements

This work is supported by the Laboratory-Directed Research and Development Program (LDRD) of the Pacific Northwest National Laboratory (PNNL) and by the U.S. Department of Energy (DOE). The NMR work was carried out at the Environmental and Molecular Sciences Laboratory, a national scientific user facility sponsored by the DOE's Office of Biological and Environmental Research (BER) and located at PNNL. PNNL is a multiprogram laboratory operated by Battelle Memorial Institute for the Department of Energy under Contract DE-AC05-76RL01830.

Appendix A. Supplementary data

Supplementary data associated with this article can be found, in the online version, at doi:10.1016/j.jpowsour.2010.09.060.

References

[1] J. Xu, C. Jia, B. Cao, W.F. Zhang, Electrochim. Acta 52 (2007) 8044–8047.
[2] A.R. Armstrong, G. Armstrong, J. Canales, P.G. Bruce, J. Power Sources 146 (2005) 501–506.
[3] J. Kim, J. Cho, J. Electrochem. Soc. 154 (2007) A542–A546.
[4] E. Ferg, R.J. Gummow, A. de Kock, M.M. Thackeray, J. Electrochem. Soc. 141 (1994) L147–L150.
[5] K.M. Colbow, J.R. Dahn, R.R. Haering, J. Power Sources 26 (1989) 397–402.
[6] T. Ohzuku, A. Ueda, N. Yamamoto, J. Electrochem. Soc. 142 (1995) 1431–1435.
[7] K. Ariyoshi, R. Yamato, T. Ohzuku, Electrochim. Acta 51 (2005) 1125–1129.
[8] S. Panero, P. Reale, F. Ronci, B. Scrosati, P. Perfetti, V. Rossi Albertini, Phys. Chem. Chem. Phys. 3 (2001) 845–847.
[9] K. Nakahara, R. Nakajima, T. Matsushima, H. Majima, J. Power Sources 117 (2003) 131–136.
[10] H. Ge, N. Li, D. Li, C. Dai, D. Wang, J. Phys. Chem. C 113 (2009) 6324–6326.
[11] J. Shu, J. Solid State Electrochem. 13 (2009) 1535–1539.
[12] Z.Y. Zhong, C.Y. Ouyang, S.Q. Shi, M.S. Lei, ChemPhysChem 9 (2008) 2104–2108.
[13] P.P. Prosini, R. Mancini, L. Petrucci, V. Contini, P. Villano, Solid State Ionics 144 (2001) 185–192.
[14] K.-C. Chou, W.H. Qiu, K. Wu, G.H. Zhang, Rare Metals 25 (2006) 399–406.
[15] K. Zaghib, M. Simoneau, M. Armand, M. Gauthier, J. Power Sources 81–82 (1999) 300–305.
[16] Y.-H. Rho, K. Kanamura, J. Solid State Chem. 177 (2004) 2094–2100.
[17] Y.-J. Hao, Q.-Y. Lai, D.-Q. Liu, Z.-U. Xu, X.-Y. Ji, Mater. Chem. Phys. 94 (2005) 382–387.
[18] T. Yuan, K. Wang, R. Cai, R. Ran, Z. Shao, J. Alloys Compd. 477 (2009) 665–672.
[19] M.W. Raja, S. Mahanty, M. Kundu, R.N. Basu, J. Alloys Compd. 468 (2009) 258–262.
[20] S.Y. Yin, L. Song, X.Y. Wang, M.F. Zhang, K.L. Zhang, Y.X. Zhang, Electrochim. Acta 54 (2009).
[21] G. Wang, J. Xu, M. Wen, R. Cai, R. Ran, Z. Shao, Solid State Ionics 179 (2008).
[22] A. Deschanvres, B. Raveau, Z. Sekkal, Mat. Res. Bull. 6 (1971) 699–704.
[23] K. Kataoka, Y. Takahashi, N. Kijima, J. Akimoto, K.-I. Ohshima, J. Phys. Chem. Solids 69 (2008) 1454–1456.
[24] S. Scharner, W. Weppner, P. Schmid-Beurmann, J. Electrochem. Soc. 146 (1999) 857–861.
[25] M. Wagemaker, D.R. Simon, E.M. Kelder, J. Schoonman, C. Ringpfeil, U. Haake, D. Lützenkirchen-Hecht, R. Frahm, F.M. Mulder, Adv. Mater. 18 (2006) 3169–3173.
[26] F. Ronci, P. Reale, B. Scrosati, S. Panero, V. Rossi Albertini, P. Perfetti, M. di Michiel, J.M. Merino, J. Phys. Chem. B 106 (2002) 3082–3086.
[27] M. Wagemaker, E.R.H. Van Eck, A.P.M. Kentgens, F.M. Mulder, J. Phys. Chem. B 113 (2009) 224–230.
[28] C. Pecharromán, J.M. Amarilla, Phys. Rev. B 62 (2000) 12062–12068.
[29] I.A. Leonidov, O.N. Leonidova, L.A. Perelyaeva, R.F. Samigullina, S.A. Kovyazina, M.V. Patrakeev, Phys. Solid State 45 (2003) 2183–2188.
[30] M. Wilkening, W. Iwaniak, J. Heine, V. Epp, A. Kleinert, M. Behrens, G. Nuspl, W. Bensch, P. Heitjans, Phys. Chem. Chem. Phys. 9 (2007) 6199–6202.
[31] M. Wilkening, R. Amade, W. Iwaniak, P. Heitjans, Phys. Chem. Chem. Phys. 9 (2007) 1239–1246.
[32] M. Vijayakumar, S. Kerisit, Z. Yang, G.L. Graff, J. Liu, J.A. Sears, S.D. Burton, K.M. Rosso, J. Hu, J. Phys. Chem. C 113 (2009) 20108–20116.
[33] M. Vijayakumar, Y. Inaguma, W. Mashiko, M.-P. Crosnier-Lopez, C. Bohnke, Chem. Mater. 16 (2004) 2719–2724.
[34] Y.-J. Hao, Q.-Y. Lai, J.-Z. Lu, H.-L. Wang, Y.-D. Chen, X.-Y. Ji, J. Power Sources 158 (2006) 1358–1364.
[35] M. Kakihana, M. Tada, M. Shiro, V. Petrykin, M. Osada, Y. Nakamura, Inorg. Chem. 40 (2001) 891–894.
[36] D. Massiot, F. Fayon, M. Capron, I. King, S. Le Calvé, B. Alonso, J.-O. Durand, B. Bujoli, Z. Gan, G. Hoatson, Magn. Reson. Chem. 40 (2002) 70–76.
[37] M. Born, K. Huang, Dynamical Theory of Crystal Lattices, Oxford University Press, Oxford, UK, 1954.
[38] M. Matsui, M. Akaogi, Mol. Simul. 6 (1991) 239–244.
[39] B.G. Dick, A.W. Overhauser, Phys. Rev. 112 (1958) 90–103.
[40] S. Kerisit, N.A. Deskins, K.M. Rosso, M. Dupuis, J. Phys. Chem. C 112 (2008) 7678–7688.
[41] W. Smith, T.R. Forester, I.T. Todorov, Daresbury Laboratory, United Kingdom, 2009.
[42] K. Kataoka, Y. Takahashi, N. Kijima, H. Hayakawa, J. Akimoto, K.-I. Ohshima, Solid State Ionics 180 (2009) 631–635.
[43] W.G. Hoover, Phys. Rev. A 31 (1985) 1695–1697.
[44] S. Melchionna, G. Ciccotti, B.L. Holian, Mol. Phys. 78 (1993) 533–544.
[45] P.P. Ewald, Ann. Phys. 64 (1921) 253–287.
[46] P.J. Mitchell, D. Fincham, J. Phys.: Condens. Matter 5 (1993) 1031–1038.
[47] J.P. Kartha, D.P. Tunstall, J.T.S. Irvine, J. Solid State Chem. 152 (2000) 397–402.
[48] P. Krtil, J. Dědeček, T. Kostlánová, J. Brus, Electrochem. Solid-State Lett. 7 (2004) A163–A166.
[49] T. Kostlánová, J. Dědeček, P. Krtil, Electrochim. Acta 52 (2007) 1847–1856.
[50] M. Wagemaker, E.R.H. van Eck, A.P.M. Kentgens, F.M. Mulder, J. Phys. Chem. B 113 (2009) 224–230.
[51] Z. Xu, J.F. Stebbins, Solid State Nucl. Magn. Res. 5 (1995) 103–112.
[52] O.B. Lapina, D.F. Khabibulin, K.V. Romanenko, Z. Gan, M.G. Zuev, V.N. Krasil'nikov, V.E. Fedorov, Solid State Nucl. Magn. Res. 28 (2005) 204–224.
[53] X. Xue, J.F. Stebbins, Phys. Chem. Mineral. 20 (1993) 297–307.
[54] I. Leonidov, O. Leonidova, L. Perelyaeva, R. Samigullina, S. Kovyazina, M. Patrakeev, Phys.Solid State 45 (2003) 2183–2188.
[55] A.M. George, J.F. Stebbins, Am. Mineral. 80 (1995) 878–884.
[56] A.D. Bain, Chemical exchange, in: Annual Reports on Nmr Spectroscopy, vol. 63, Elsevier Academic Press Inc., San Diego, 2008, pp. 23–48.
[57] S. Hayashi, H. Hatano, J. Ceram. Soc. Jpn. 102 (1994) 378–382.
[58] W.J.H. Borghols, M. Wagemaker, U. Lafont, E.M. Kelder, F.M. Mulder, J. Am. Chem. Soc. 131 (2009) 17786–17792.
[59] Z. Xu, J.F. Stebbins, Science 270 (1995) 1332–1334.
[60] D. Chandler, J. Chem. Phys. 68 (1978) 2959–2970.
[61] R.W. Impey, P.A. Madden, I.R. McDonald, J. Phys. Chem. 87 (1983) 5071–5083.